

Supplementary Material:

" The Constitución earthquake of 25 March 2012: a large aftershock of the Maule earthquake near the bottom of the seismogenic zone"

This online file contains precisions about our inversions, like the geometry of the slab, the preferred models of teleseismic and InSAR/GPS inversion and the distortion due to depth phases in our back projection model.

Geometry of the slab interface in the area of the 2012 Constitución earthquake. **Figure S1** shows geometry of the slab interface in the area of the 2012 Constitución earthquake derived from different slab models.

Rupture Velocity Test. In order to test the stability and robustness of the solution, we perform the kinematic inversion for P and S waves, varying the rupture velocity from 1.2 to 2.7 km/s, each 0.5 km/s. The results of those tests are in **Figure S2**. All of these models produce almost identical source time functions (see figure 4) and very similar average rake values $\approx 100^\circ$. The data fit from each solution are pretty good (residual variance less than 0.2).

Back projection distortion due to depth phases. We interpret northwards-trending peaks in the back projection (BP) analysis (**Figure S3**) as artifacts due to depth phases (pP and sP). To support this statement, we modeled the P-pP-sP wave train associated to the P_2 hypocenter at one central station of the US network (KSU1 – shown in red on Figure 2A), and we compared the timing of the northwards-trending peaks with the arrival time of pP and sP phases. Modeling of teleseismic P-waves is performed using ray methods (Okal, 1992), for the AK135 global velocity model (Kennet et al. 1995); the takeoff angles of P, pP and sP phases were computed using the TauP code (Crotwell et al., 1999). We used the focal mechanism proposed by the USGS Centroid Moment Solution (strike = 12° , dip = 19° , rake = 101°). Depth was fixed to 28 km after some trial-and-error qualitative fits between modeled and observed data. The bottom panel in **Figure S4** shows simple modeling of teleseismic displacement at station KSU1 where the effects of focal mechanism, surface reflectivity, relative P and S amplitude at the source, and anelastic attenuation ($Q_p = 1500$) are taken into account. Middle panel is the synthetic trace convolved for a triangle source time function with rise time of 2 sec, differentiated to velocity, and convolved for the instrumental response. This synthetic trace matches reasonably well the observed velocity signal on the BHZ component at station KSU1. Arrivals corresponding to BP peaks – p12s through p20s (shown in **Figure S4**) – are reported on the observed trace. They are all associated to the arrival of depth phases, as shown by our modeling. We choose, therefore, to exclude these points from our analysis.

Resolution tests for joint InSAR/GPS inversion. In order to assess the capacity of the inversion scheme to constrain the main features of the slip distribution, we compared slip distributions obtained for various degrees of smoothing (**Figure S5**, top row). A typical "L-curve" is obtained when plotting the final magnitude and RMS misfit to the data versus solution roughness (see Jónsson et al., 2001). This curve highlights the trade-off between imposed degree of smoothing and fit-to-the data. Horizontal dashed lines in **Figure S5** (top row) indicate the minimum RMS misfit achieved by the inversion of either the InSAR data only ("min RMS InSAR") or the GPS data only ("min RMS GPS"). The joint

inversion yields a fit-to-the data close to that obtained by either the GPS-only or the InSAR-only inversions, which demonstrates that the solution is well constrained by the two independent data sets. We also computed the resolution power and the restitution power of the inversion (**Figure S5**, middle and bottom rows). The resolution and the restitution quantify the accuracy in the reconstruction of an imposed slip distribution after inversion of the synthetic data set produced by that imposed slip distribution. For each patch, the synthetic slip distribution is chosen as a unit slip on the current patch and zero slip elsewhere. The resolution quantifies how much that unit slip is attributed to the right patch. The resolution indicates how much the imposed unit slip is spread on neighbouring patches. It mostly depends on the magnitude of the smoothing constraint. On the other hand, the **restitution** gives, for each patch, the total magnitude of the slip integrated over the fault plane after inverting the synthetic data produced by a unit slip distribution. The restitution is useful to assess how much slip can be under- or over-estimated in different areas of the fault plane. A **restitution** greater (smaller) than one on a given patch means that slip occurring on that patch would be over-estimated (under-estimated) by the inversion (see Radiguet et al., 2011). Two particular solutions are highlighted in **Figure S5**. Solution A corresponds to the "optimal" solution in the sense of the L-curve criterion. However, the restitution for solution A is not uniform over the fault plane, with a maximum greater than one at the centre of the fault plane and minima smaller than one near the edges. This means that the slip distribution will be excessively spread across the fault plane, and that any slip occurring near the fault edges will be severely attenuated by the inversion. Hence, solution A is considered to correspond to excessive smoothing. Solution B is the "preferred" solution. The restitution is nearly uniformly equal to one, except on a few patches located offshore. The slip distribution is relatively compact, with a clear peak slip and two minor local slip maxima.

Figure Captions.

Figure S1. Geometry of the slab interface in the area of the 2012 Constitución earthquake derived from slab models (Tassara et al., 2006 - solid line; Hayes et al., 2012 - dashed line), seismicity recorded by a local network (Campos et al., 2002 - circles) and receiver functions (Dannowski et al., 2013 - stars). The fault plane used in this study is indicated by the rectangular area in the top figure.

Figure S2. Finite source model of the 2012 Constitución earthquake from the teleseismic inversion of P and S waves using different rupture velocities. Slip distribution on the fault is shown by the circles colored following the scale shown at the bottom, white and black stars indicate the P1 and P2 hypocenters, respectively. The black rectangle represents the fault area used in the inversion.

Figure S3. Back projection peaks for the Constitución earthquake. Peaks plotted with discontinuous border are considered to be due to pP and sP depth phases, and are labeled according to their timing with respect to the event origin time.

Figure S4. Simple teleseismic modeling of the P-pP-sP wave train at station KSU1 (shown in red on Figure 2A). *Bottom panel:* displacement trace including the effect of source excitation, reflection at the surface and anelastic attenuation. *Middle panel:* synthetic trace convolved for a triangular source with 2 s rise time, differentiated to velocity and convolved with the instrument response. *Top panel:* observed velocity at BHZ component. Traces are normalized to their maximum amplitude. P1 is the observed direct P-wave arrival time from the first hypocenter. P2, pP2 and sP2 are theoretical arrival times for direct P-wave and depth phases from the second hypocenter. p12s – p20s are arrival times corresponding to the back projection peaks shown in figure S4.

Figure S5. Resolution tests for the joint InSAR and GPS static inversion. Top panel: trade-off between imposed smoothing, final magnitude and RMS misfit to the data. Middle and bottom panels: slip distribution (left), resolution (middle) and restitution (right) for two particular solutions (A: “optimal”; B: “preferred”).

References:

- Campos, J., Hatzfeld, D., Madariaga, Lopez, G., Kausel, E., Zollo, A., Barrientos, S. and Lyoncaen H., 2002, The 1835 seismic gap in South Central Chile, *Phys. Earth Planet. Int.* , 132, 177-195.
- Crotwell, H. P., T. J. Owens, and J. Ritsema, 1999. The TauP Toolkit: Flexible seismic travel-time and ray-path utilities, *Seismological Research Letters* 70, 154–160.
- Dannowski, A., Grevemeyer, I., Kraft, H. A., Arroyo, I. and Thorwart, M. (2013) Crustal thickness and mantle wedge structure from receiver functions in the Chilean Maule region at 35° S *Tectonophysics* . DOI 10.1016/j.tecto.2013.02.015.
- Hayes, G. P., D. J. Wald, and R. L. Johnson (2012), Slab1.0: A three-dimensional model of global subduction zone geometries, *J. Geophys. Res.*, 117, B01302, doi:10.1029/2011JB008524.
- Jónsson, S., H. Zebker, P. Segall, and F. Amelung, 2002. Fault Slip Distribution of the 1999 Mw7.1 Hector Mine Earthquake, California, estimated from Satellite Radar and GPS Measurements, *Bull. Seismol. Soc. Am.*, 92, 1377-1389.
- Kennett, B.L.N., Engdahl, E.R., Buland, R. 1995. Constraints on seismic velocities in the Earth from traveltimes. *Geophys. J. Int.*, 122(1), 108–124. doi: 10.1111/j.1365-246X.1995.tb03540.x.
- Okal, E.A. 1992. A student’s guide to teleseismic body wave amplitudes. *Seismol Res Lett*, 63, 169–180.
- Radiguet, M., F. Cotton, M. Vergnolle, M. Campillo, B. Valette, V. Kostoglodov, and N. Cotte, 2011, Spatial and temporal evolution of a long term slow slip event: the 2006 Guerrero Slow Slip Event, *Geophys. J. Int.*, 184 (2), 816-828.
- Tassara, A., Götze, H.-J., Schmidt, S., Hackney, R. (2006). Three-dimensional density model of the Nazca plate and the Andean continental margin, *Journal of Geophysical Research*, 111, B09404, doi:10.1029/2005JB003976.

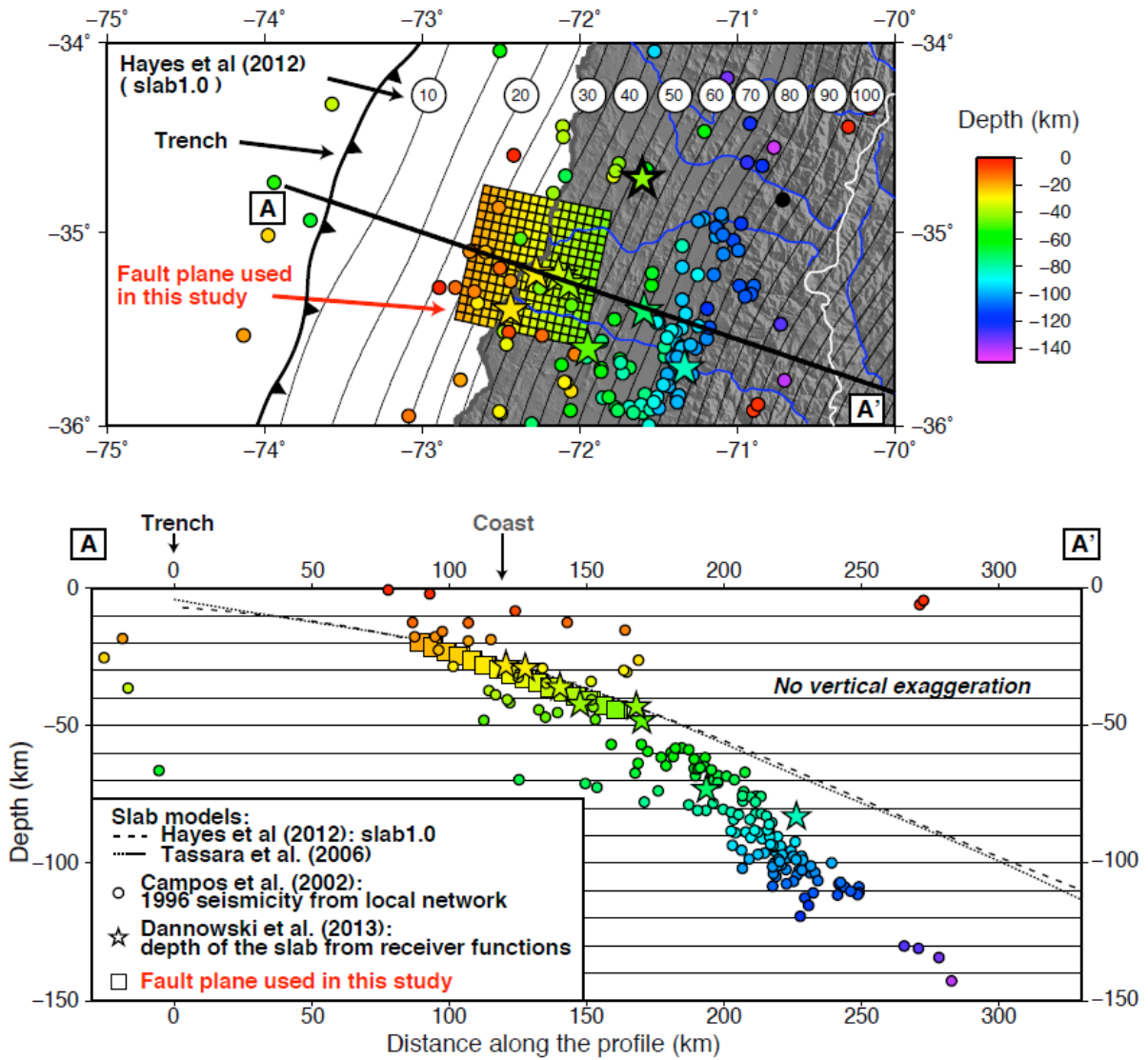


Figure S1. Geometry of the slab interface in the area of the 2012 Constitución earthquake derived from slab models (Tassara et al., 2006 - solid line; Hayes et al., 2012 - dashed line), seismicity recorded by a local network (Campos et al., 2002 - circles) and receiver functions (Dannowski et al., 2013 - stars). The fault plane used in this study is indicated by the rectangular area in the top figure.

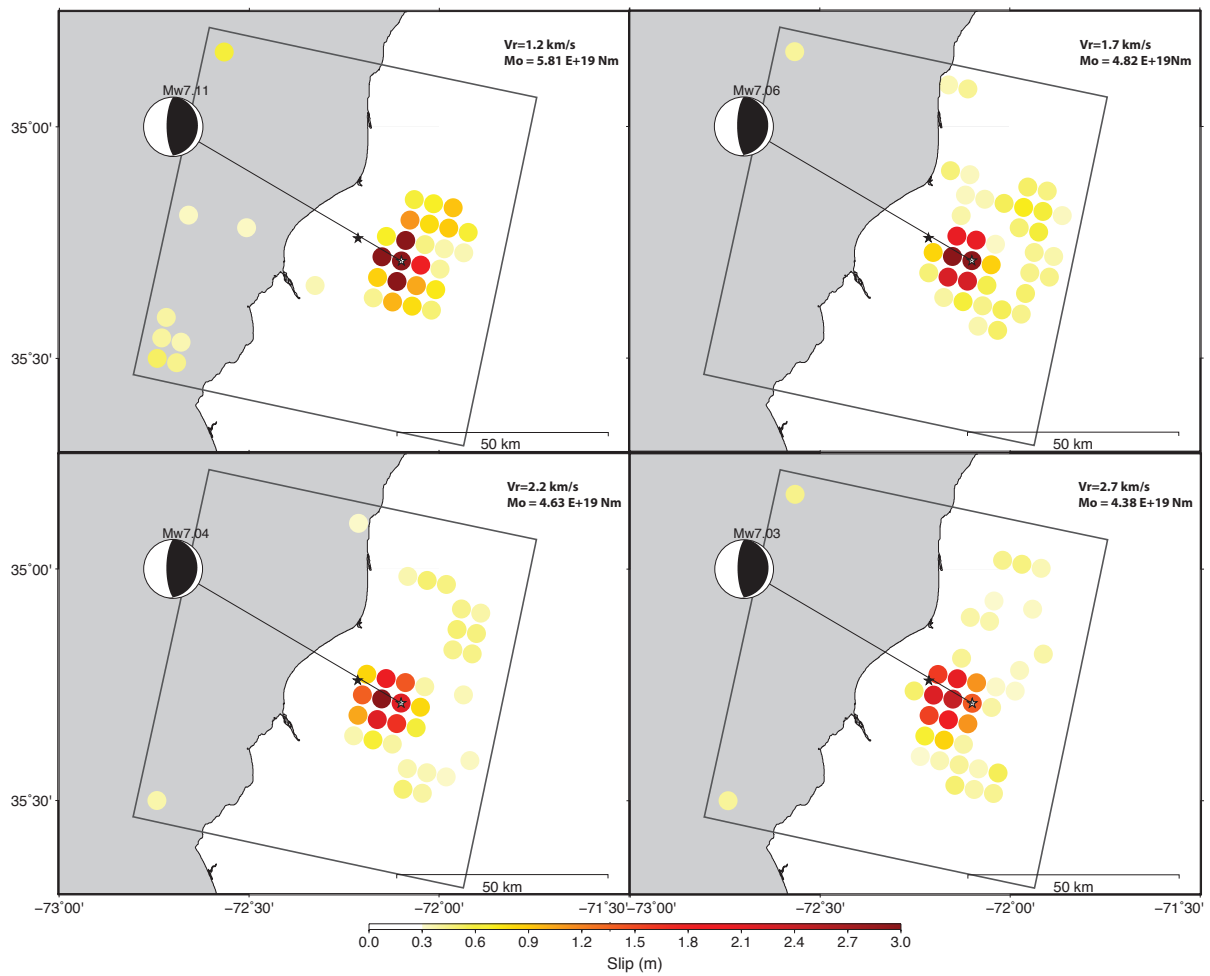


Figure S2. Finite source model of the 2012 Constitución earthquake from the teleseismic inversion of P and S waves using different rupture velocities. Slip distribution on the fault is shown by the circles colored following the scale shown at the bottom, white and black stars indicate the P1 and P2 hypocenters, respectively. The black rectangle represents the fault area used in the inversion.

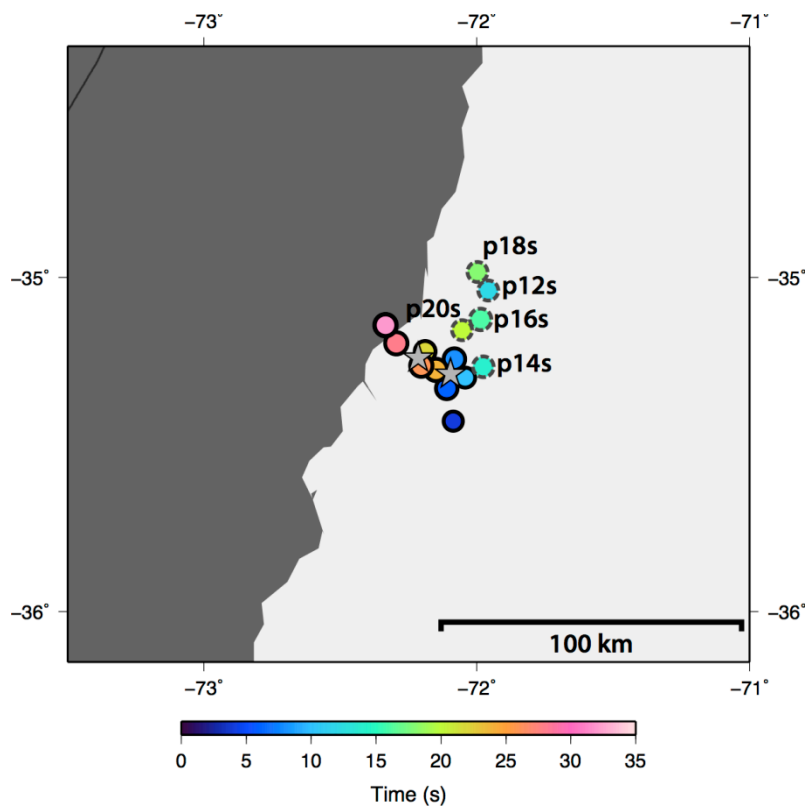


Figure S3. Back projection peaks for the Constitución earthquake. Peaks plotted with discontinuous border are considered to be due to pP and sP depth phases, and are labeled according to their timing with respect to the event origin time.

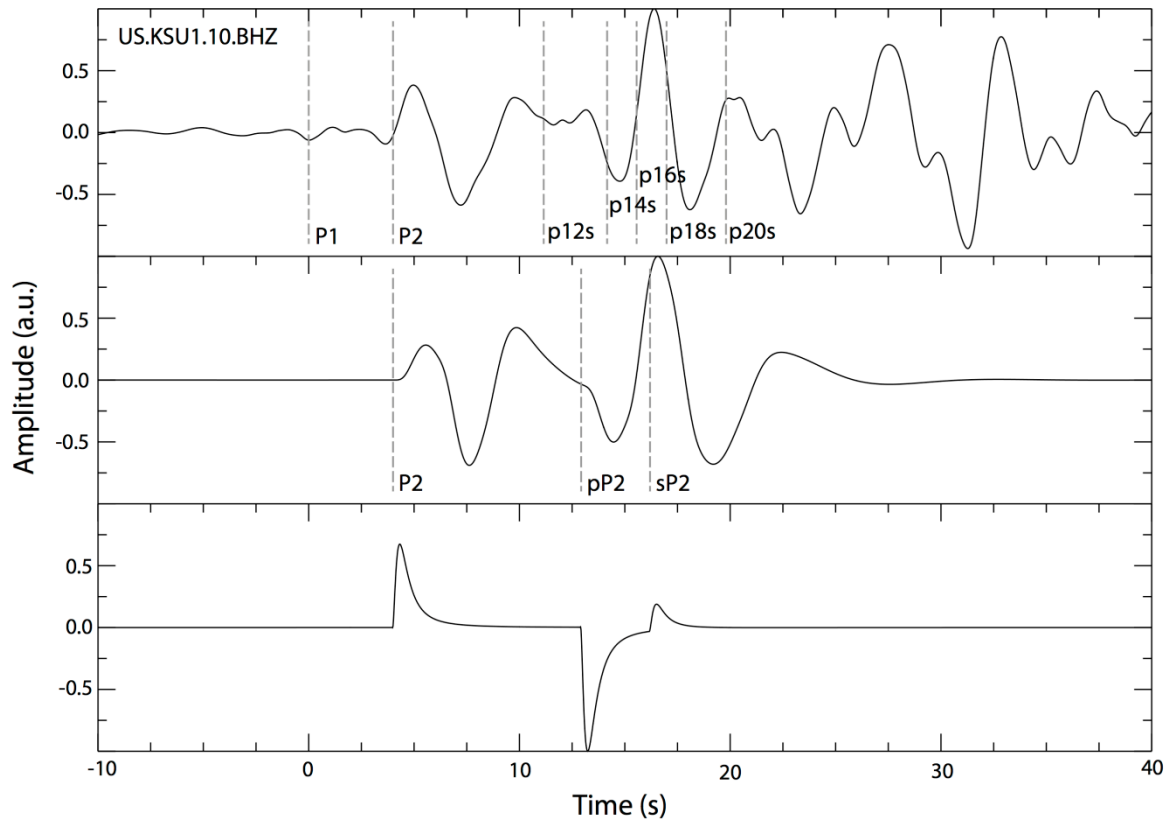


Figure S4. Simple teleseismic modeling of the P-pP-sP wave train at station KSU1 (shown in red on Figure 2A). *Bottom panel:* displacement trace including the effect of source excitation, reflection at the surface and anelastic attenuation. *Middle panel:* synthetic trace convolved for a triangular source with 2 s rise time, differentiated to velocity and convolved with the instrument response. *Top panel:* observed velocity at BHZ component. Traces are normalized to their maximum amplitude. P1 is the observed direct P-wave arrival time from the first hypocenter. P2, pP2 and sP2 are theoretical arrival times for direct P-wave and depth phases from the second hypocenter. p12s – p20s are arrival times corresponding to the back projection peaks shown in figure S4.

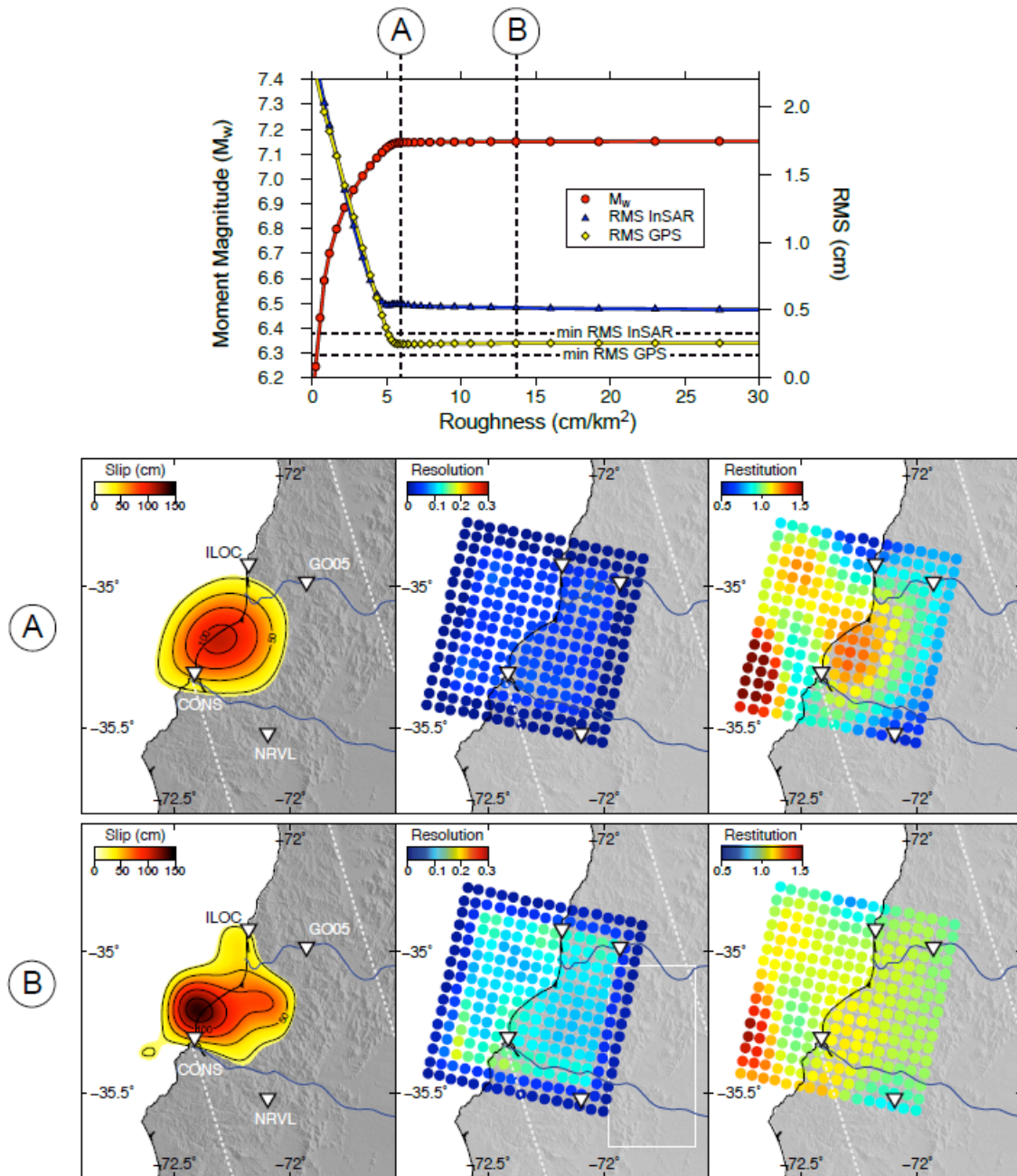


Figure S5. Resolution tests for the joint InSAR and GPS static inversion. Top panel: trade-off between imposed smoothing, final magnitude and RMS misfit to the data. Middle and bottom panels: slip distribution (left), resolution (middle) and restitution (right) for two particular solutions (A: “optimal”; B: “preferred”).